Electronic Supplementary Material (ESI) for Faraday Discussions.

Probing assembly/disassembly of ordered molecular hydrogels

Susana Ramalhete[1], Karol Nartowski[1,2 ^], Hayley Green[3], Jesús Angulo[4], Dinu Iuga[5], László Fábián[1], Gareth O. Lloyd[6] and Yaroslav Z. Khimyak[1, 2]

[1]*School of Pharmacy, University of East Anglia, Norwich Research Park, Norwich, NR2 1TS, United Kingdom*
[2]*Department of Drug Form Technology, Wroclaw Medical University, Borowska 211A, 50-556 Wroclaw, Poland*
[3]*Institute of Chemical Sciences, School of Engineering and Physical Sciences, Heriot-Watt University, Edinburgh, United Kingdom, EH14 4AS*
[4]*Instituto de Investigaciones Químicas (CSIC-US), Avda. Américo Vespucio, 49, Sevilla 41092, Spain*
[5]*Department of Physics, University of Warwick, CV4 7AL, Coventry, United Kingdom*
[6]*School of Chemistry, University of Lincoln, Lincoln, LN6 7DL, United Kingdom*
^Deceased author

SUPPLEMENTARY INFORMATION

Table of contents

1. Molar ratio and concentration

Table S1. Molar ratio and **c**oncentration of Phe and NH_2-Phe in suspensions and hydrogels under study.

Molar ratio	[Phe] (mM)	[NH_2-Phe] (mM)
Phe	303	0
1:0.05	303	15
1:0.1	303	30
1:0.15	303	45
1:0.2	303	60
1:0.3	303	90
1:0.4	303	120
1:1	303	303
1:2	303	606
NH_2-Phe	0	606

2. Thermal properties of hydrogels

Gel-to-solution transition temperature (T_{gel}) reflects the thermal energy needed to break non-covalent interactions responsible for holding the supramolecular network together.[1] It is therefore a useful indicator of fibre strength and stability of intermolecular interactions.[1]

Table S2. Gel-to-solution transition temperature (T_{gel}) of Phe (303 mM), Phe/NH_2-Phe (1:2) and NH_2-Phe (606 m) hydrogels.

	T_{gel} range / K
Phe	324 – 327
Phe/NH_2-Phe (1:2)	319 – 324
NH_2-Phe	317 – 320

3. Single crystal X-ray diffraction

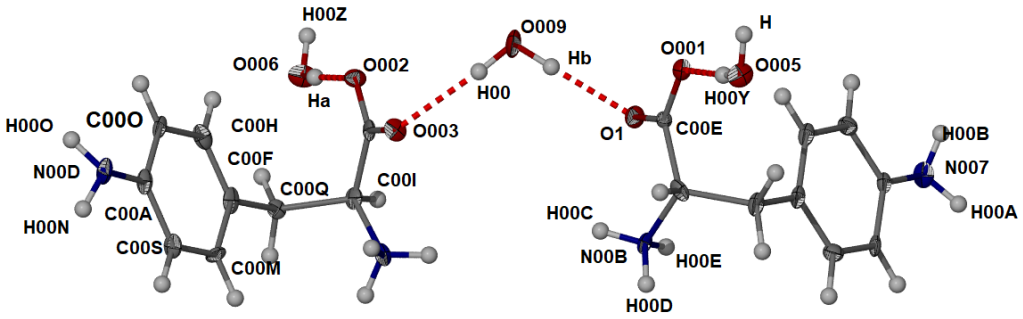

Figure S1. Ellipsoid plot of the asymmetric unit of the $(NH_2\text{-Phe})_2(H_2O)_3$ crystal structure obtained from the hydrogel materials.

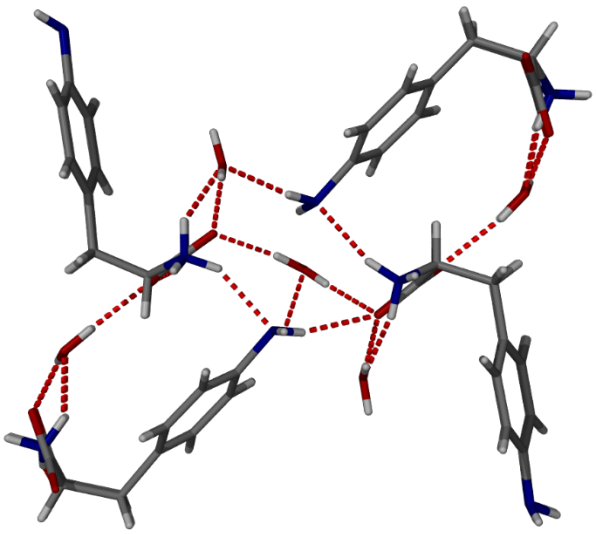

Figure S2. Component of the packing of the $(NH_2\text{-Phe})_2(H_2O)_3$ crystal structure showing the extensive hydrogen bonding present in the structure.

Further analysis of the crystal packing was performed within the crystallographic software Crystal Explorer. The packing was compared with that of the $(Phe)_2(H_2O)_2$ crystal structure (our own published data, GOFWOP02). To perform the analyses the structures' hydrogen positions were normalised using Mercury (CCDC). Those CIFs were then analysed utilising the Crystal Explorer software and Tonto (single point molecular wavefunction at B3LYP/6-31G(d,p)). Interaction map calculations were performed and the following data represents the results of the analyses. Scale factors utilised for total energies, which is the sum of the four energy components, are 1.057 k_col, 0.740 k_pol, 0.871 k_dis, and 0.618 k_rep.

$(Phe)_2(H_2O)_2$ crystal structure energy framework analysis.

Table S3. $(Phe)_2(H_2O)_2$ crystal structure molecule-to-molecule interaction energies. Distance represents the distance between the molecular centroids (mean atomic position).

N	Symmetry operations	Distance (Å)	E_{Coul}	E_{Pol}	E_{Disp}	E_{Rep}	**E_{tot}**
1	-	3.30	-32.4	-13.1	-11.4	39.2	**-29.7**
0	-	3.02	-20.7	-4.5	-2.9	16.5	**-17.6**
0	-	2.85	-36.7	-7.5	-2.9	35.6	**-24.8**
1	x, y, z	5.41	-112.6	-37.0	-27.4	72.7	**-125.3**
1	-	5.21	-151.0	-37.6	-30.1	73.9	**-168.1**
1	-x, y+1/2, -z	6.99	-28.8	-26.9	-13.3	31.2	**-42.6**
1	-x, y+1/2, -z	7.88	0.2	-0.5	-9.1	3.7	**-5.9**
1	-	9.94	-1.6	-0.3	-6.1	2.8	**-5.5**
0	-	5.54	-64.3	-16.0	-4.5	63.0	**-44.8**
0	-	4.91	-74.8	-18.7	-7.3	55.4	**-65.0**
0	-	4.91	-74.8	-18.7	-7.3	55.4	**-65.0**
0	-	6.28	-2.9	-5.0	-5.1	5.0	**-8.1**
0	x, y, z	5.41	-115.2	-39.5	-33.2	88.2	**-125.5**
0	-x, y+1/2, -z	6.54	-1.7	-1.1	-20.6	12.6	**-12.7**

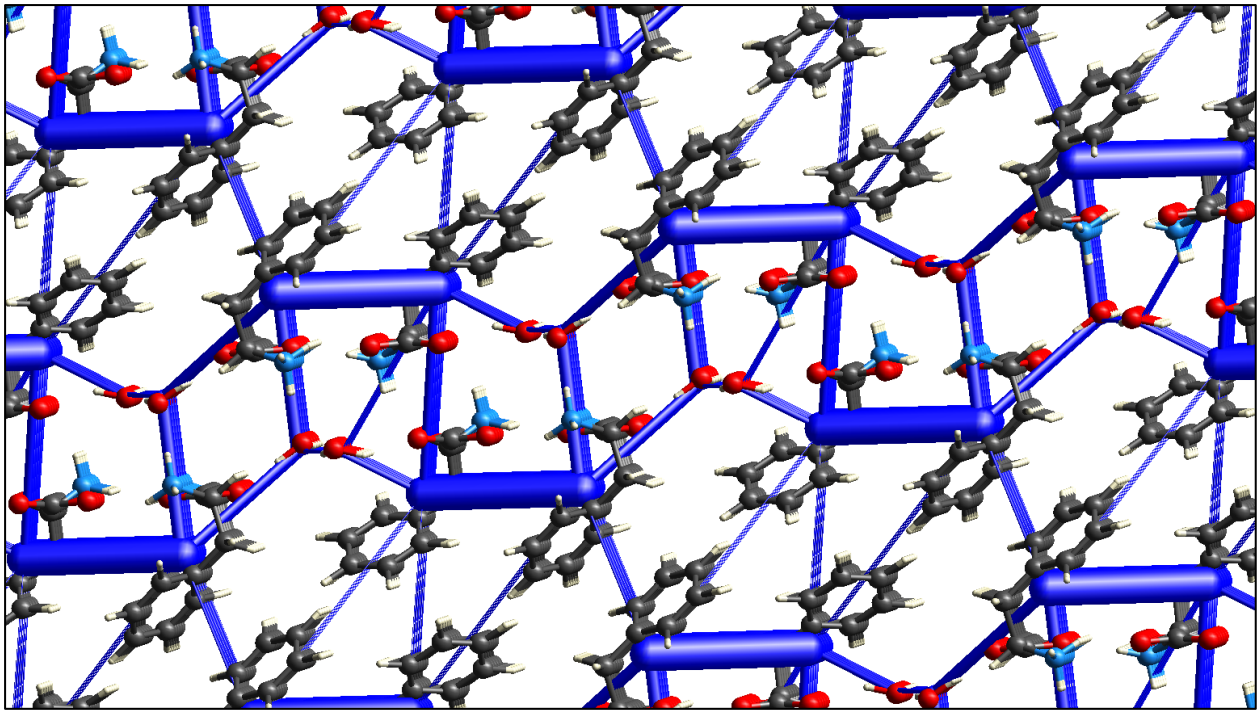

Figure S3. $(Phe)_2(H_2O)_2$ crystal structure packed and showing the energy framework. The tube size (scale factor) used in all the energy frameowrks was 50. Structure viewed down the b-axis.

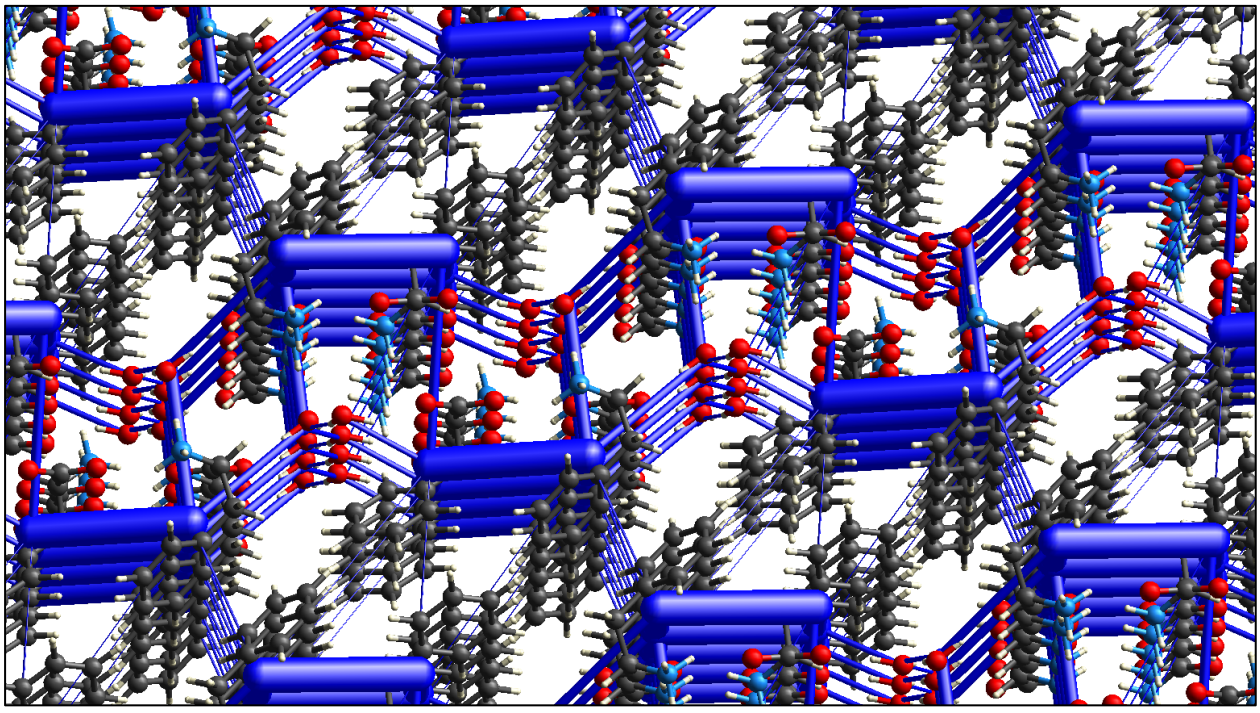

Figure S4. $(Phe)_2(H_2O)_2$ crystal structure packed and showing the energy framework. The tube size (scale factor) used in all the energy frameworks was 50. Structure viewed down the b-axis, but slightly tilted. This allows for a better view of the strongest interaction that corresponds to the stacking of the zwitterion groups.

$(NH_2\text{-Phe})_2(H_2O)_3$ Energy Framework analysis.

Table S4. NH_2-Phe to NH_2-Phe interactions.

N	Symmetry operations	Distance (Å)	E_{Coul}	E_{Pol}	E_{Disp}	E_{Rep}	$\mathbf{E_{tot}}$
0	x, y, z	5.98	-107.2	-32.1	-24.6	69.6	**-115.6**
1	x, y, z	5.98	-106.0	-28.7	-24.5	72.1	**-110.1**
0	-	5.29	-1.4	-3.1	-44.9	33.3	**-22.3**
0	-x, y+1/2, -z	6.16	-68.2	-21.2	-30.5	42.2	**-88.2**
0	-	8.74	-20.8	-12.3	-10.0	18.3	**-28.5**
2	-x, y+1/2, -z	6.22	-64.3	-22.7	-31.9	53.0	**-79.7**
1	-	8.78	-12.2	-7.7	-9.1	6.5	**-22.5**

Table S5. Water interactions with NH_2-Phe molecules.

N	Symmetry operations	Distance (Å)	E_{Coul}	E_{Pol}	E_{Disp}	E_{Rep}	$\mathbf{E_{tot}}$
0	-	5.55	-32.0	-11.3	-5.3	32.4	**-26.7**
1	-	5.57	-38.5	-12.5	-4.7	41.6	**-28.5**
0	-	6.52	-11.6	-2.9	-4.0	9.6	**-11.9**
0	-	5.64	-18.8	-5.7	-5.7	9.1	**-23.4**
0	-	4.47	-30.1	-10.6	-4.6	25.6	**-27.9**
0	-	4.66	-60.3	-16.8	-9.2	48.7	**-54.1**
0	-	3.83	-28.0	-8.8	-8.5	22.2	**-29.8**
0	-	6.32	-11.5	-2.2	-3.8	4.2	**-14.5**
0	-	4.47	-30.1	-10.6	-4.6	25.6	**-27.9**
0	-	4.66	-60.3	-16.8	-9.2	48.7	**-54.1**
1	-	6.32	-11.5	-2.2	-3.8	4.2	**-14.5**
0	-	3.83	-28.0	-8.8	-8.5	22.2	**-29.8**
0	-	6.52	-11.6	-2.9	-4.0	9.6	**-11.9**
0	-	5.64	-18.8	-5.7	-5.7	9.1	**-23.4**
1	-	4.11	-28.4	-10.8	-6.6	30.2	**-25.1**
0	-	4.70	-61.4	-16.8	-9.0	52.1	**-53.0**
0	-	6.23	-24.8	-5.1	-4.7	18.7	**-22.5**
0	-	3.96	-33.4	-9.3	-6.9	23.5	**-33.7**

0	-	4.11	-28.4	-10.8	-6.6	30.2	**-25.1**
0	-	4.70	-61.4	-16.8	-9.0	52.1	**-53.0**
0	-	6.23	-24.8	-5.1	-4.7	18.7	**-22.5**
1	-	3.96	-33.4	-9.3	-6.9	23.5	**-33.7**

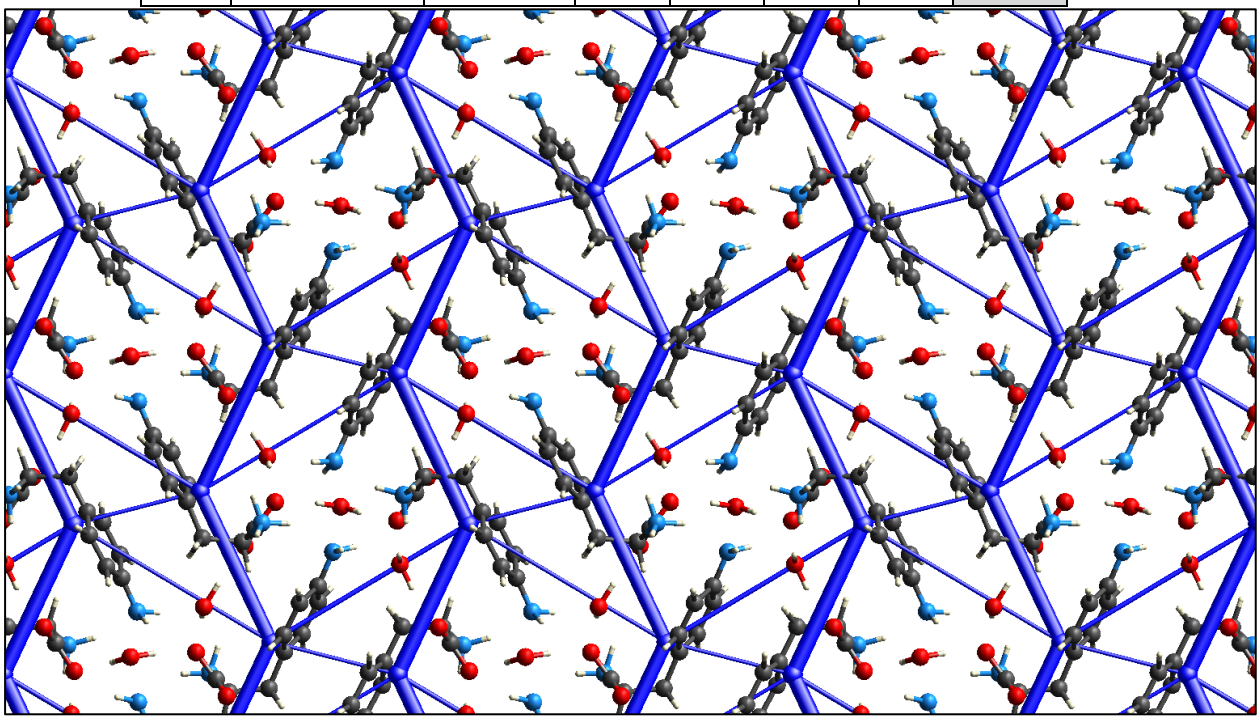

Figure S5. $(NH_2\text{-Phe})_2(H_2O)_3$ energy framework of only the NH_2-Phe molecules viewed down a-axis.

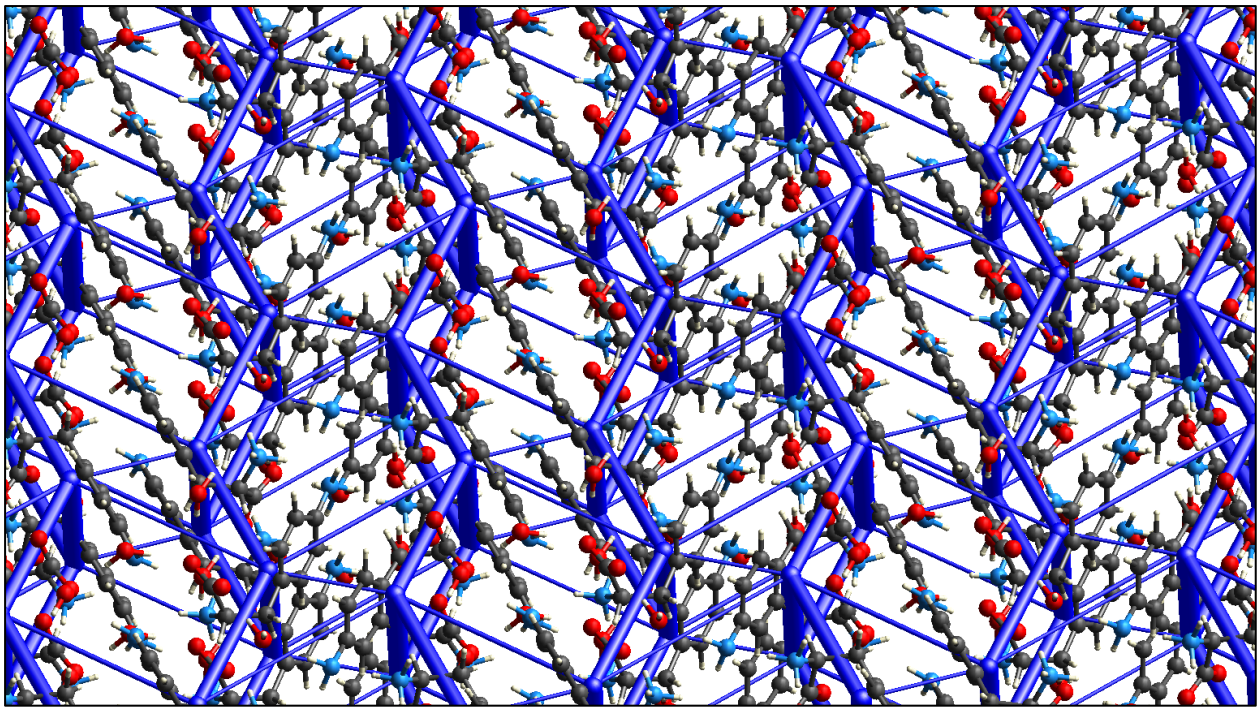

Figure S6. $(NH_2\text{-Phe})_2(H_2O)_3$ energy framework of only the NH_2-Phe molecules viewed down the slightly titled a-axis. This allows for viewing of the stacking zwitterion groups.

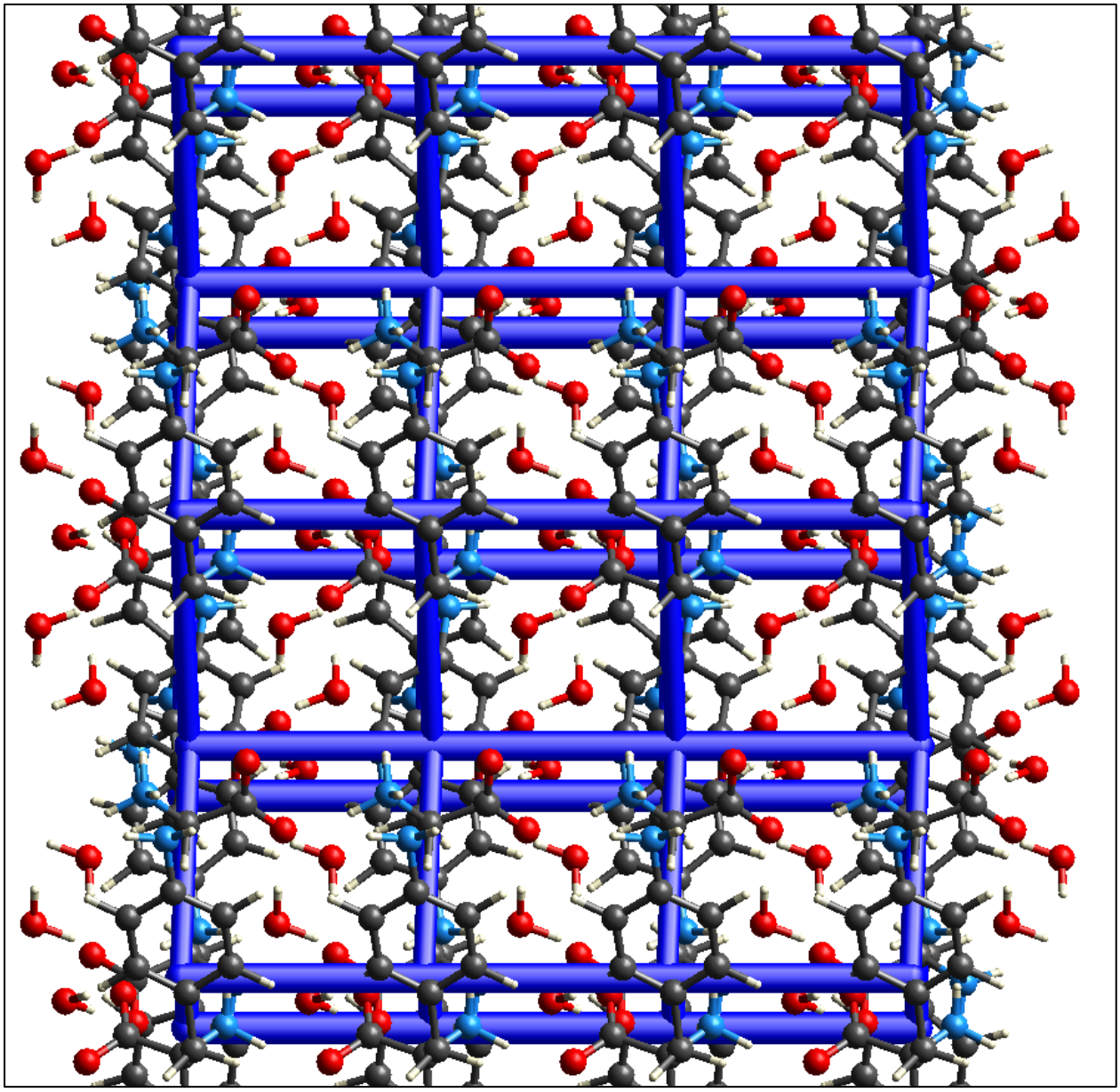

Figure S7. $(NH_2\text{-Phe})_2(H_2O)_3$ energy framework of only the NH_2-Phe molecules viewed down c-axis.

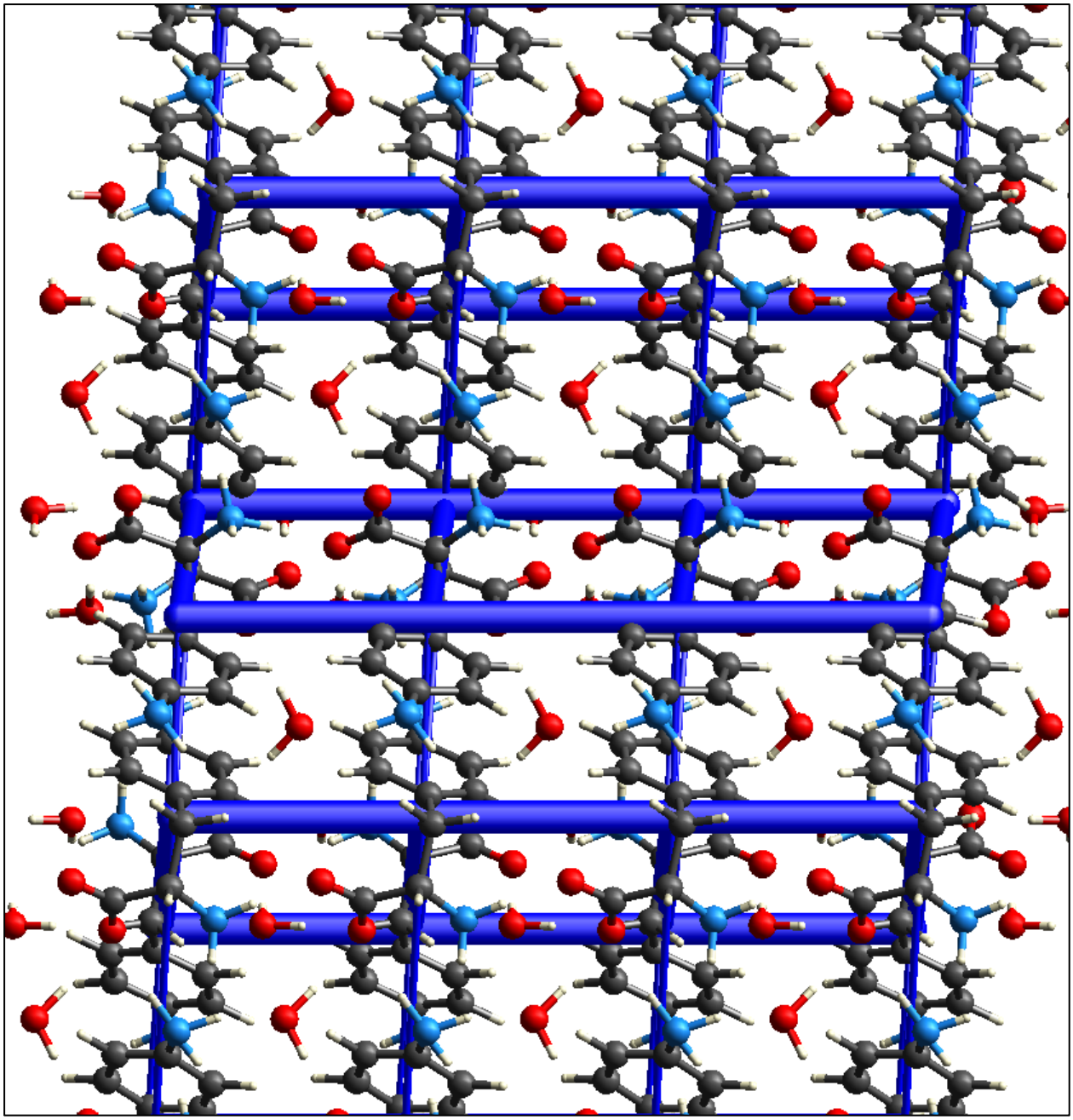

Figure S8. $(NH_2\text{-Phe})_2(H_2O)_3$ energy framework of only the NH_2-Phe molecules viewed down b-axis

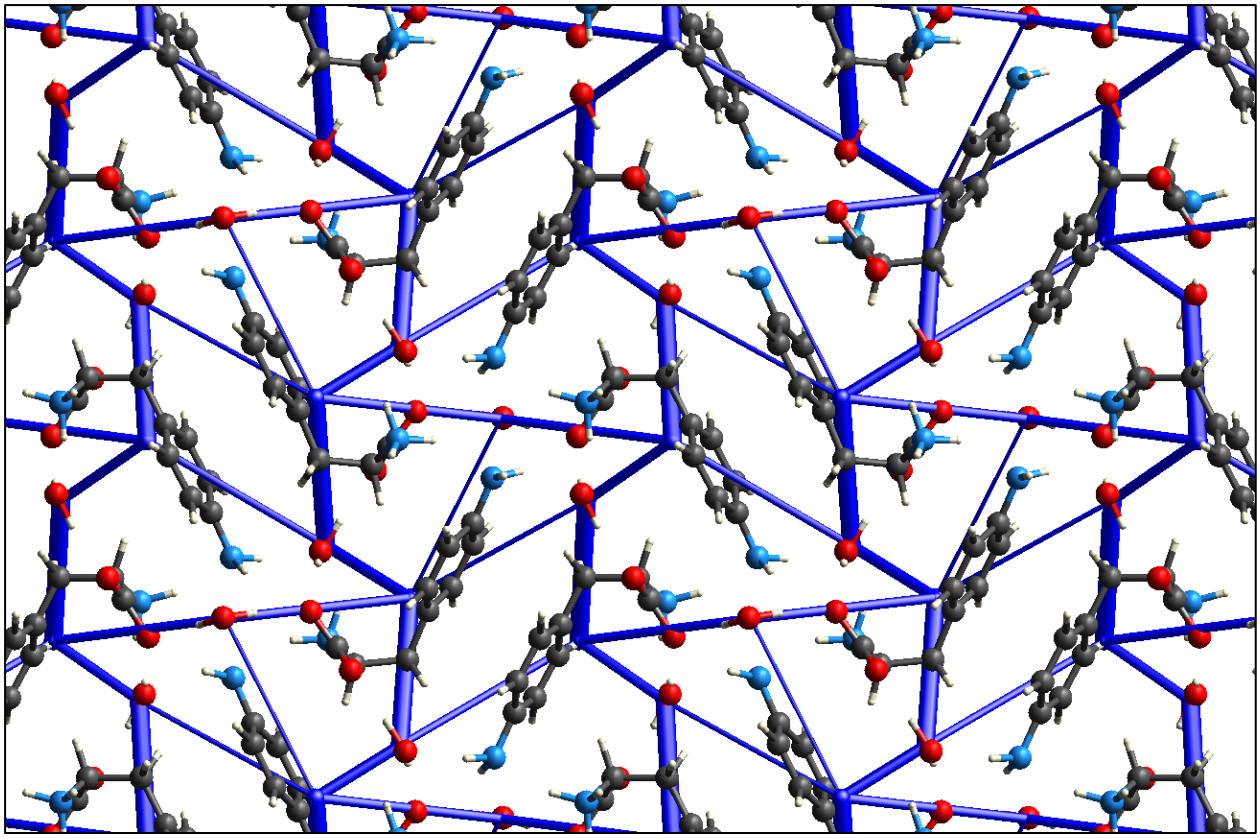

Figure S9. $(NH_2\text{-Phe})_2(H_2O)_3$ energy framework of the water molecules viewed down the a-axis.

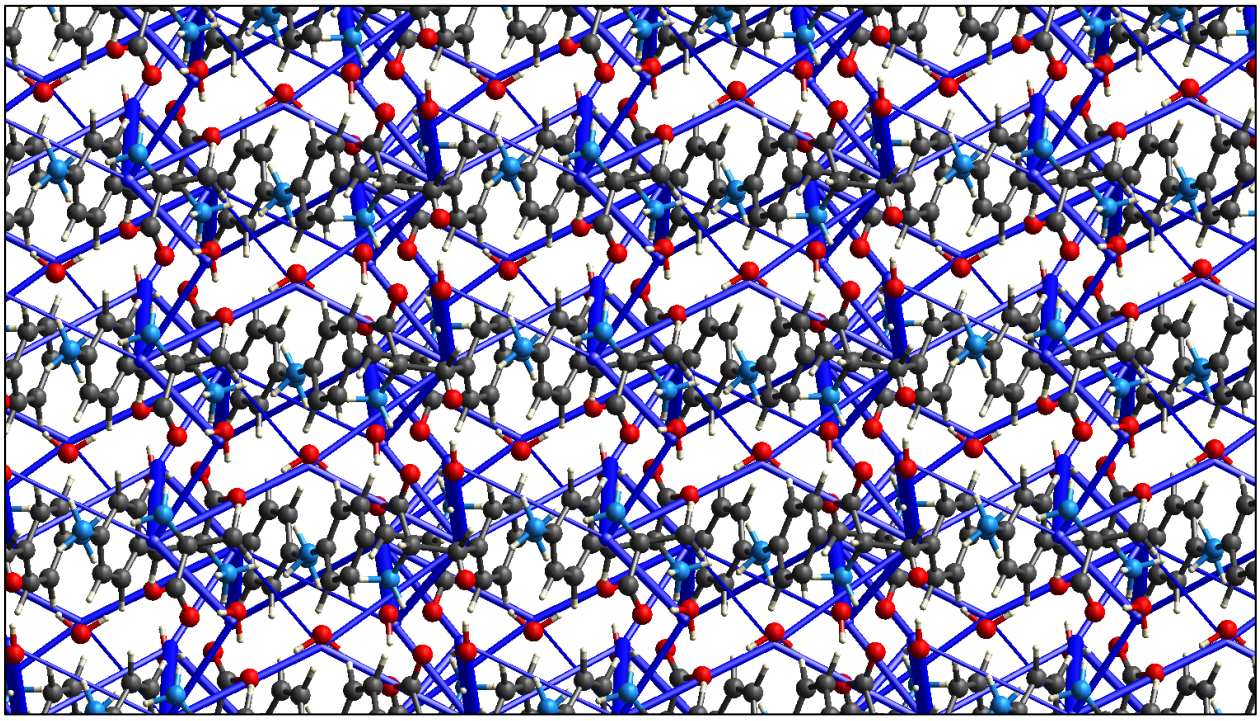

Figure S10. $(NH_2\text{-Phe})_2(H_2O)_3$ energy framework of the water molecules viewed down the b-axis. There are no clear "preferential" interactions.

Morphology determination from the $(NH_2\text{-}Phe)_2(H_2O)_3$ crystal structure

Having the atomic details of the $(NH_2\text{-}Phe)_2(H_2O)_3$ crystal structure allows us to assess the morphology prediction utilising the BFDH process applied within Mercury.

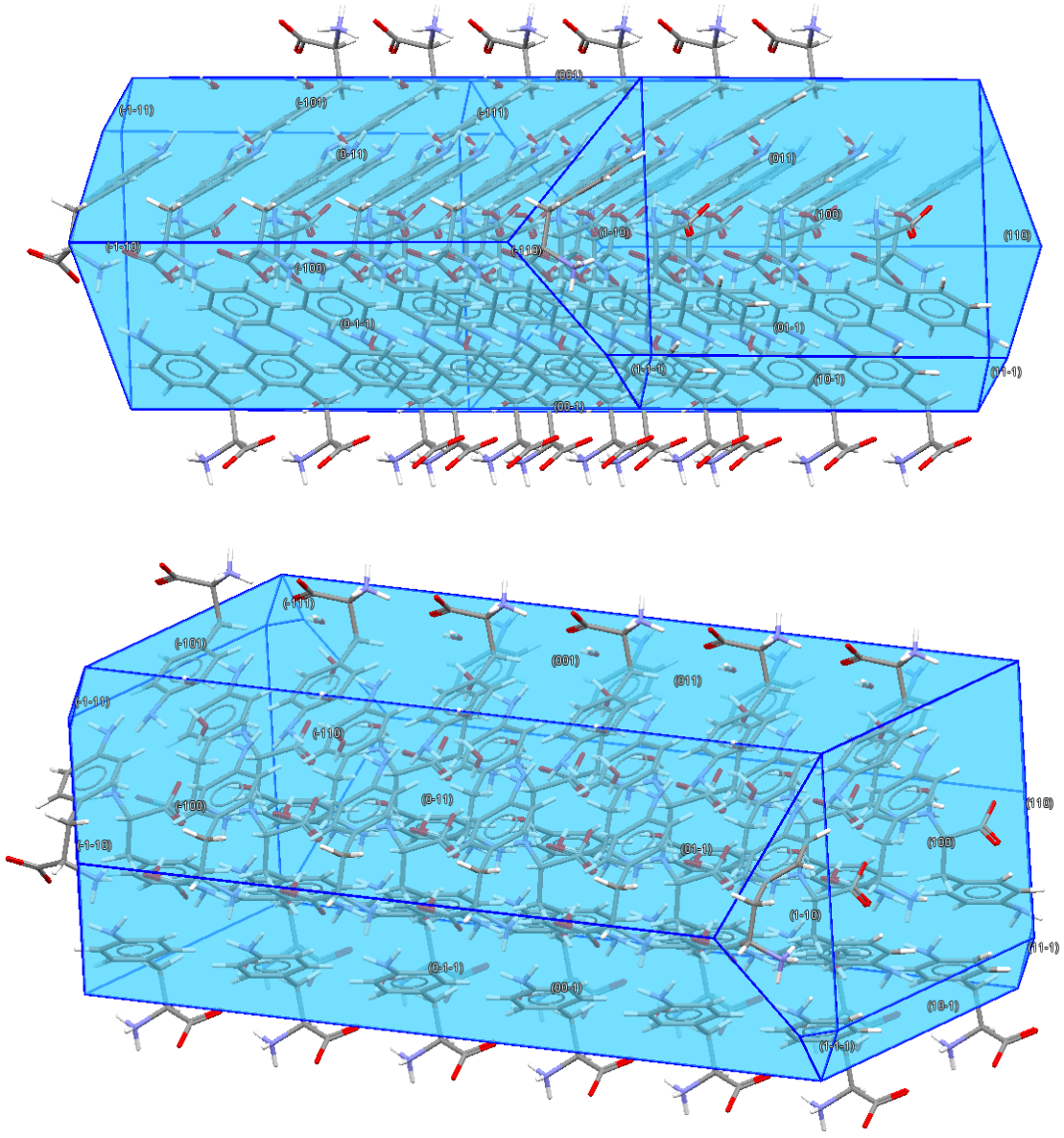

Figure S11. BFDH morphology prediction of $(NH_2\text{-}Phe)_2(H_2O)_3$ showing that the growing faces (100) and (-100) also matches the strong electrostatic interaction between the zwitterion groups. The larger, and therefore slower growing faces, consist of aryl functionality and the hydrogen bonding associated with the amino groups, water and the zwitterion groups.

4. Powder X-Ray diffraction

Drying the hydrogels under vacuum did not affect their tridimensional crystalline organisation, as the diffraction distances of PXRD patterns acquired with wet and dried hydrogel samples were similar.

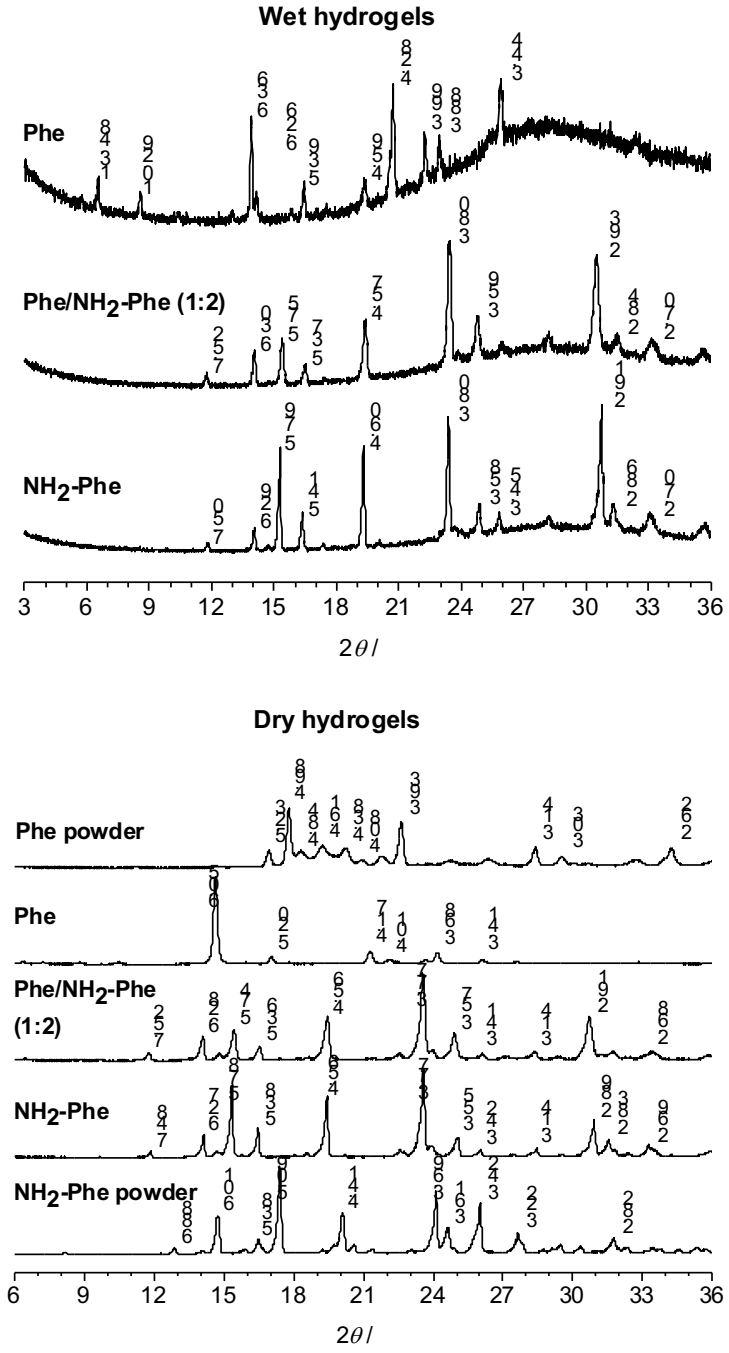

Figure S11. PXRD patterns of reference solid powders of the anhydrous form I of Phe and commercially available NH_2-Phe; and of Phe, Phe/NH_2-Phe (1:2) and NH_2-Phe wet and dry hydrogel samples.

A good agreement was found between the powder pattern calculated from the single crystal data and the experiment collected pattern from a hydrogel sample. There are differences (shift along the 2θ axis and peak intensities) due to some preferred orientation that could not be modelled and temperature difference of each of the data collections (room temperature for hydogel and 100K for the single crystal).

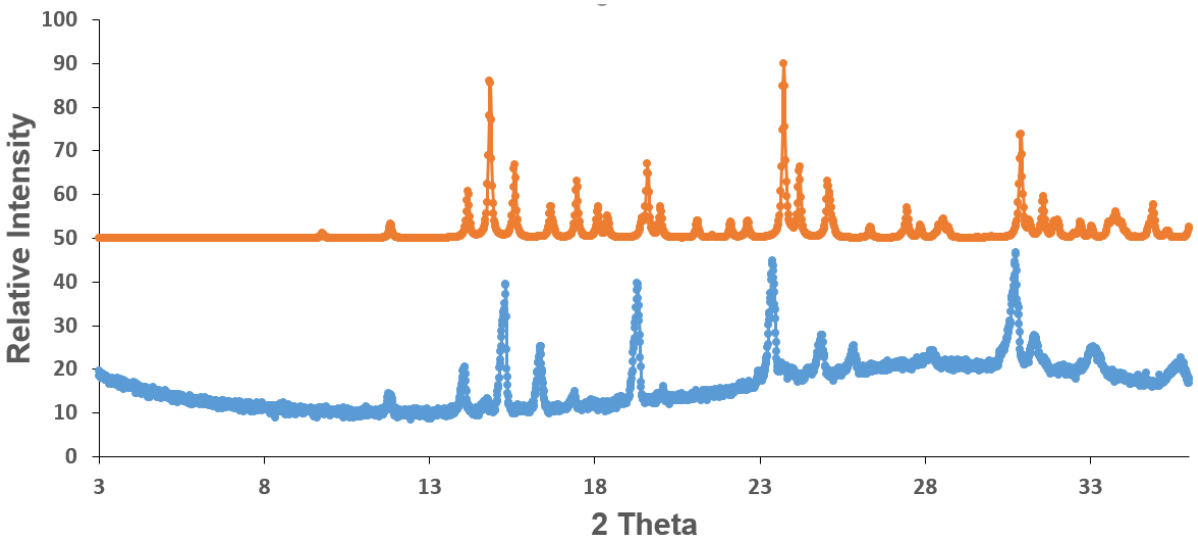

Figure S12. PXRD patterns of $(NH_2\text{-Phe})_2(H_2O)_3$ from hydrogel experiments (blue, lower pattern) vs calculated from the single crystal data (orange, top).

5. Nuclear magnetic resonance spectroscopy

5.1. Solid-state NMR spectroscopy

5.1.1. ^{1}H-^{13}C CP/MAS experiments

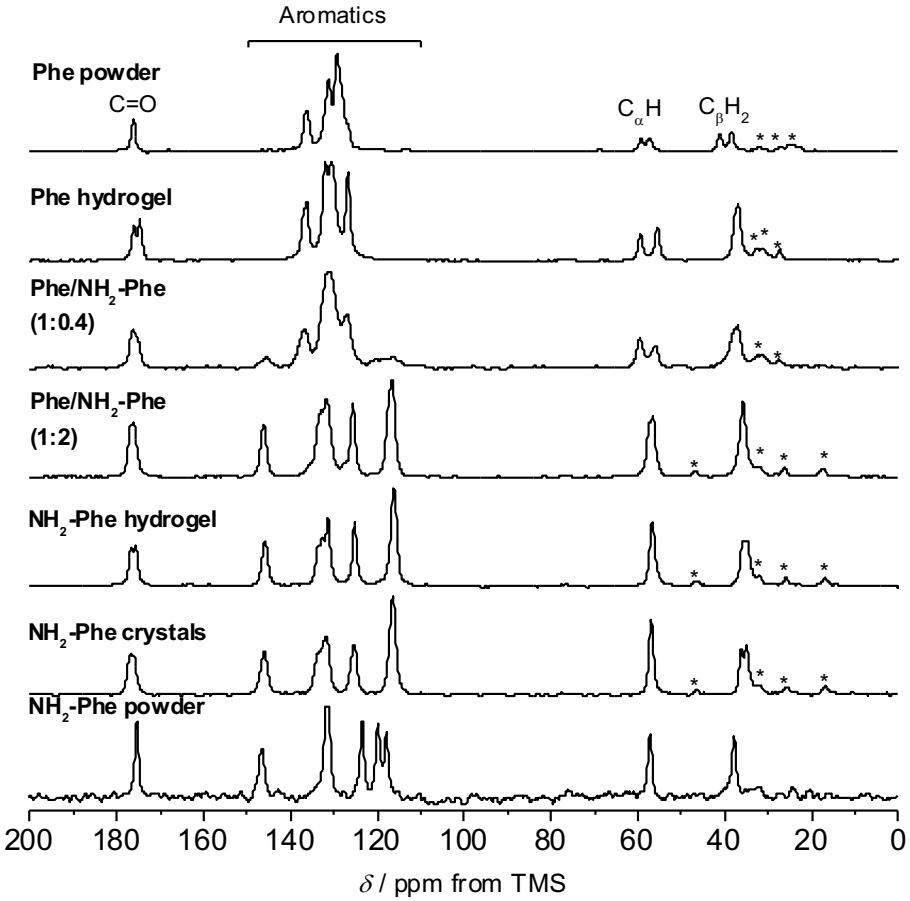

Figure S13. ^{1}H-^{13}C CP/MAS NMR spectra of reference solid powders of the anhydrous form I of Phe and commercially available NH_2-Phe; NH_2-Phe crystals; Phe, Phe/NH_2-Phe (1:2) and NH_2-Phe dry hydrogel samples; and Phe/NH_2-Phe (1:0.4) dry particles removed from suspension, acquired with an MAS rate of 10 kHz using a 400 MHz spectrometer.

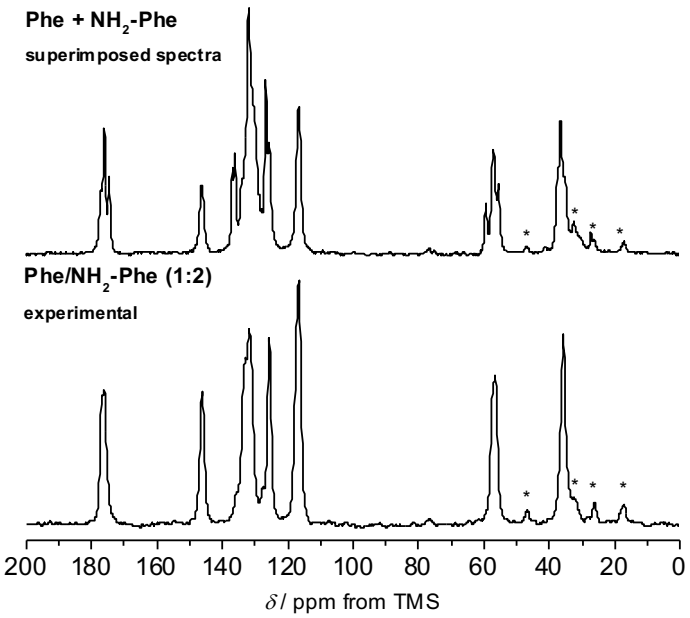

Figure S15. Experimental ^{1}H-^{13}C CP/MAS NMR spectra of Phe/NH_2-Phe (1:2) dry hydrogel sample and simulated spectra resultant from the superimposition of spectra of Phe and NH_2-Phe pure dry hydrogel samples, acquired with an MAS rate of 10 kHz using a 400 MHz spectrometer.

Table S6. ^{13}C chemical shift values (δ) from ^{1}H-^{13}C CP/MAS NMR spectra of Phe and NH_2-Phe reference solid powders and Phe (303 mM), Phe/NH_2-Phe (1:0.2), Phe/NH_2-Phe (1:0.2), Phe/NH_2-Phe (1:2) and NH_2-Phe (606 mM) dry hydrogel samples.

	^{13}C δ / ppm						
	Phe reference solid powder	Phe	Phe/NH_2-Phe (1:0.2)	Phe/NH_2-Phe (1:0.4)	Phe/NH_2-Phe (1:2)	NH_2-Phe	NH_2-Phe reference solid powder
C=O	176.07	176.01	176.11	176.30	176.84	177.09	175.32
		174.55	175.16	175.43	175.96	176.00	
C4 (NH_2-Phe)	-	-	-	145.50	146.07	146.15	146.47
C4 (Phe)	136.28	136.89	137.84	136.88	136.01	-	-
	-	136.11	136.18	-	-	134.07	131.72
	131.02	131.97	132.67	-	132.86	132.93	131.07
	129.28	130.52	130.75	130.97	131.80	131.66	-
	-	-	-	-	125.57	125.46	123.44
C1 (Phe)	126.69	126.69	126.31	126.85	127.57	-	-
C1 (NH_2-Phe)	-	-	-	116.17	116.43	116.67	119.76
							117.87
$C_\alpha H$	59.24	59.39	58.65	59.58	56.42	57.06	57.14
	57.44	55.50	56.25	55.78			
$C_\beta H_2$	41.12	37.43	37.19	38.01	35.73	36.35	37.77
	38.36	36.73	36.37	36.88		35.07	

5.2. Solution-state NMR spectroscopy

5.2.1. ^{1}H-NMR experiments

To take advantadge of the quantitative ability of ^{1}H solution-state NMR experiments, calibration curves of peak intensity ($\int$) against concentration ([]) were built for Phe and NH_2-Phe in water, and the following relationships were found:

$$\int = 7.59 \times 10^{5} \text{ [Phe]} \qquad \text{Equation S1}$$

$$\int = 6.56 \times 10^{5} \text{ [NH}_2\text{-Phe]} \qquad \text{Equation S2}$$

Taking advantage of the quantitative ability of solution-state ^{1}H-NMR, we dissolved these aggregates in DMSO-d_6 and found out Phe and NH_2-Phe were present in a 1:1 ratio.

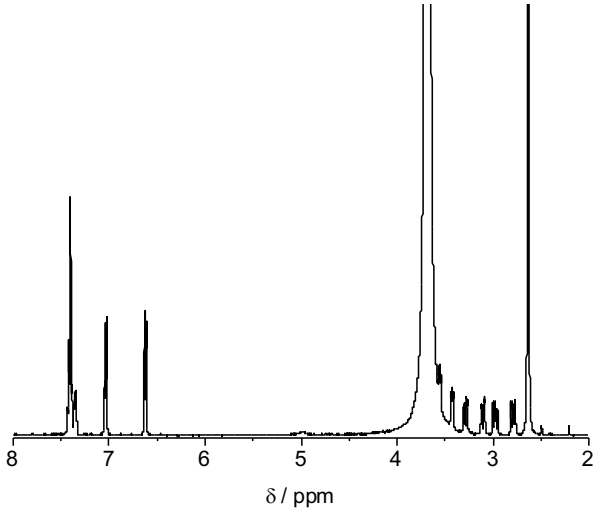

Figure S16. ^{1}H solution-state NMR spectra of Phe/NH_2-Phe (1:0.4) particles removed from suspension, dried and dissolved in DMSO-d_6.

Table S7. Percentage of dissolved gelator molecules calculated from ^{1}H solution-state NMR peak intensity according to Equations 1 and 2 for Phe (303 mM), Phe/NH_2-Phe (1:0.05), Phe/NH_2-Phe (1:0.15), Phe/NH_2-Phe (1:0.2), Phe/NH_2-Phe (1:0.55), Phe/NH_2-Phe (1:2) and NH_2-Phe (606 mM) hydrogels, measured at 298 K.

	[Phe] in solution (%)	**[NH_2-Phe] in solution (%)**
Phe	47	-
Phe/NH_2-Phe (1:0.05)	50	90
Phe/NH_2-Phe (1:0.1)	55	65
Phe/NH_2-Phe (1:0.15)	61	56
Phe/NH_2-Phe (1:0.2)	76	51
Phe/NH_2-Phe (1:0.55)	88	63
Phe/NH_2-Phe (1:2)	40	40
NH_2-Phe	-	20

5.2.2. Longitudinal relaxation time experiments

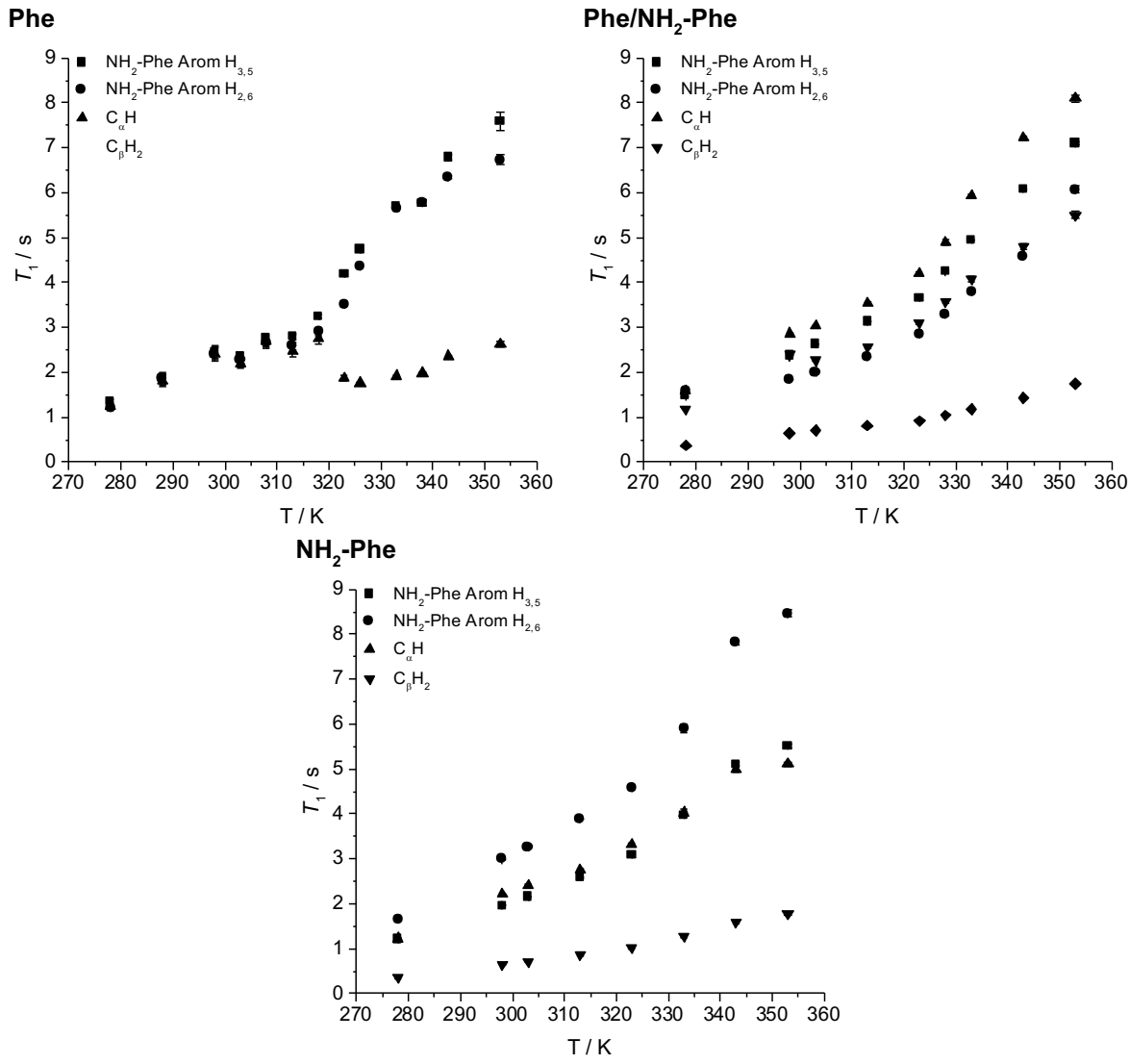

Figure S17. ^{1}H longitudinal relaxation times (T_1) for Phe Arom, NH_2-Phe Arom, $C_\alpha H$ and $C_\beta H_2$ of Phe (303 mM), Phe/NH_2-Phe (1:2) and NH_2-Phe (606 mM) hydrogels measured between 278 and 328 K.

Table S8. ^{1}H solution-state NMR longitudinal relaxation times (T_1) for Phe, Phe/NH_2-Phe (1:0.05), Phe/NH_2-Phe (1:0.1), Phe/NH_2-Phe (1:0.15), Phe/NH_2-Phe (1:0.2), Phe/NH_2-Phe (1:0.4), Phe/NH_2-Phe (1:2) and NH_2-Phe hydrogels ([Phe] = 303 mM) and Phe and NH_2-Phe solutions (101 mM) measured at 298 K, with error values in parenthesis.

	T_1 (s)						
	Arom			**$C_\alpha H$**		**$C_\beta H_2$**	
	Phe	**NH_2-Phe $H_{3,5}$**	**NH_2-Phe $H_{2,6}$**	**Phe**	**NH_2-Phe**	**Phe**	**NH_2-Phe**
Phe (solution)	2.07 (0.02)	-	-	2.20 (0.03)	-	0.63 (0.01)	-
Phe	2.45 (0.14)	-	-	2.42 (0.15)	-	2.41 (0.15)	-
Phe/NH_2-Phe (1:0.05)	2.16 (0.10)	1.88 (0.09)	1.91 (0.05)	2.14 (0.12)[a]	2.14 (0.12)[a]	2.10 (0.12)[b]	2.10 (0.09)[b]
Phe/NH_2-Phe (1:0.1)	1.94 (0.01)	1.86 (0.03)	1.95 (0.04)	1.76 (0.03)	1.68 (0.06)	1.55 (0.07)	1.26 (0.10)
Phe/NH_2-Phe (1:0.15)	1.95 (0.01)	1.82 (0.03)	2.02 (0.02)	1.89 (0.04)	1.84 (0.07)	1.30 (0.06)	1.13 (0.08)
Phe/NH_2-Phe (1:0.2)	1.98 (0.03)	1.87 (0.02)	2.15 (0.07)	1.83 (0.02)	1.74 (0.01)	1.15 (0.06)	0.81 (0.04)
Phe/NH_2-Phe (1:0.4)	2.16 (0.02)	1.77 (0.01)	2.38 (0.04)	2.34 (0.03)	2.08 (0.06)	0.70 (0.03)	0.56 (0.02)
Phe/NH_2-Phe (1:2)	1.66 (0.01)	1.26 (0.01)	1.57 (0.03)	1.53 (0.02)[c]	1.53 (0.02)[c]	0.64 (0.02)	0.59 (0.01)
NH_2-Phe	-	1.33 (0.04)	1.67 (0.04)	-	1.48 (0.03)	-	0.56 (0.05)
NH_2-Phe (solution)	-	1.96 (0.03)	3.13 (0.02)	-	2.31 (0.02)	-	0.66 (0.02)

[a, b, c] Overlapped

5.2.3. Saturation transfer difference NMR experiments

Saturation transfer difference (STD) NMR experiments were carried out to assess dynamics of exchange at the gel/solution interfaces.[2, 3] A monoexponential evolution of build-up of saturation in solution was observed in the Phe hydrogel (Figure S18), resultant from fast exchange phenomena between gel and solution states in the NMR relaxation time scale.[2] In contrast, low initial build-up values (STD_0) were observed in the NH_2-Phe pure and Phe/NH_2-Phe mixed hydrogels (Figure S19 and Figure S20). Accumulation of saturation in solution for Phe was therefore less efficient in the multiple gelator hydrogel, due to faster rate of exchange between bound and free states on the NMR relaxation time scale. VT NMR measurements were carried out to investigate exchange phenomena. The levels of accumulation of saturation in solution decreased with temperature, showing the rate of exchange between gel and solution states was becoming even faster.

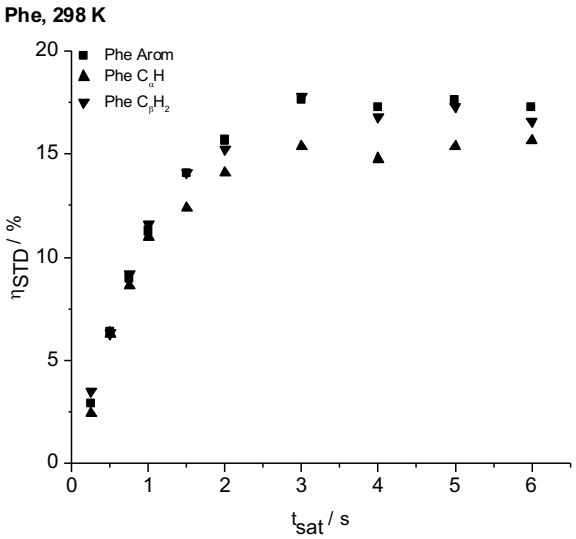

Figure S18. Evolution of fractional STD response (η_{STD}) for Phe hydrogels measured at 298 K.

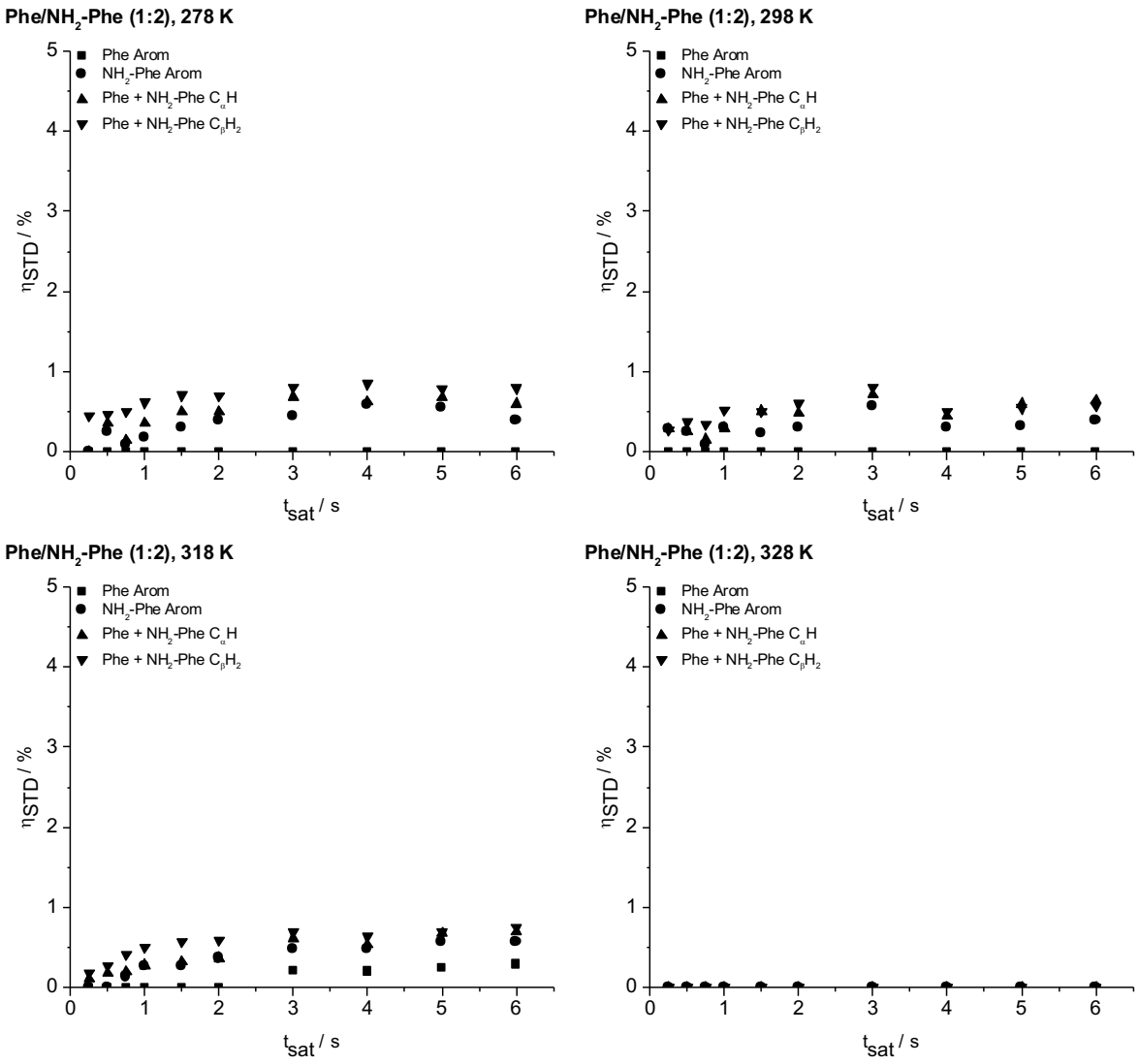

Figure S19. Evolution of fractional STD response (η_{STD}) for Phe/NH_2-Phe (1:2) hydrogels measured between 278 and 328 K.

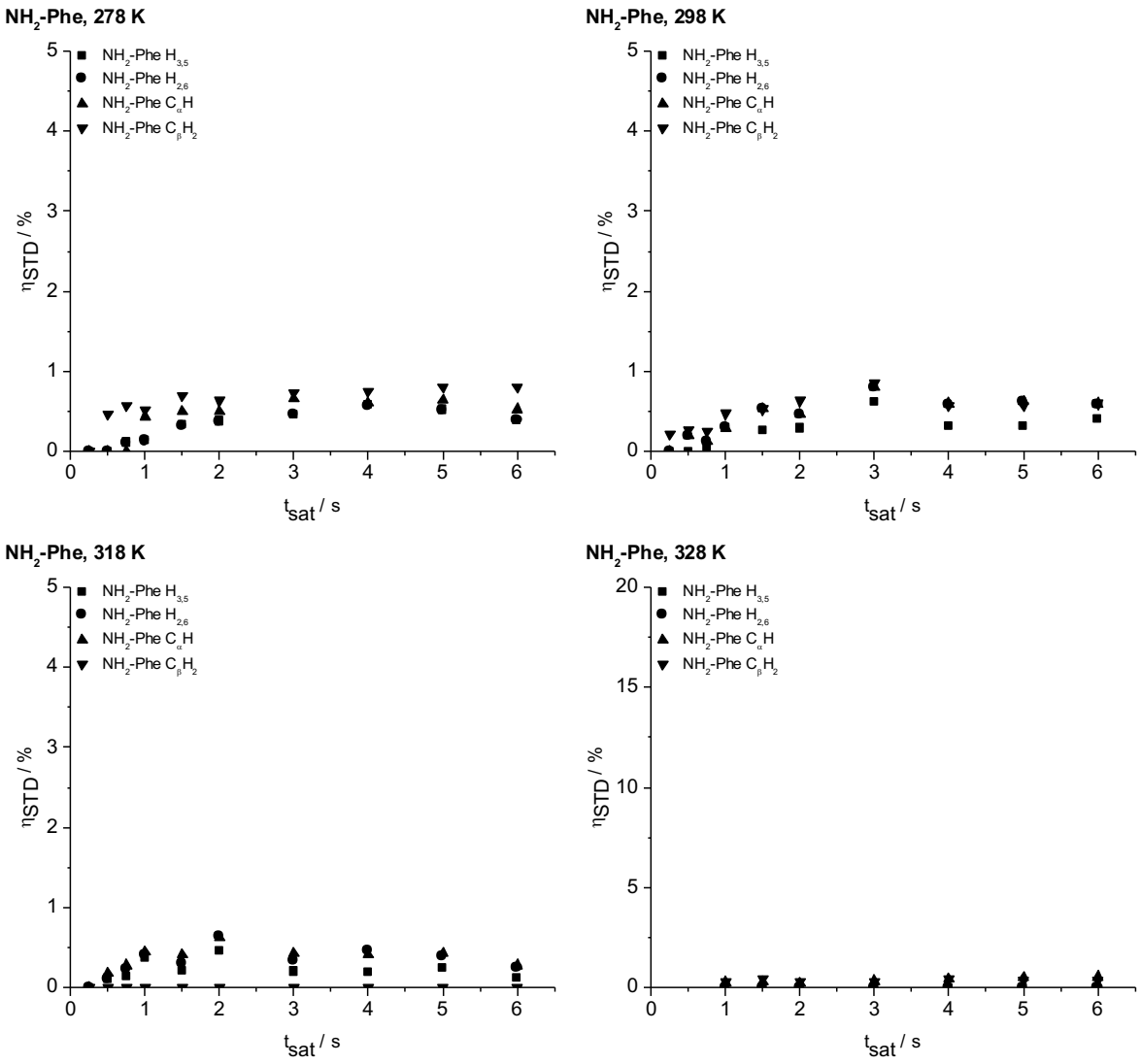

Figure S20. Evolution of fractional STD response (η_{STD}) for NH_2-Phe hydrogels measured between 278 and 328 K.

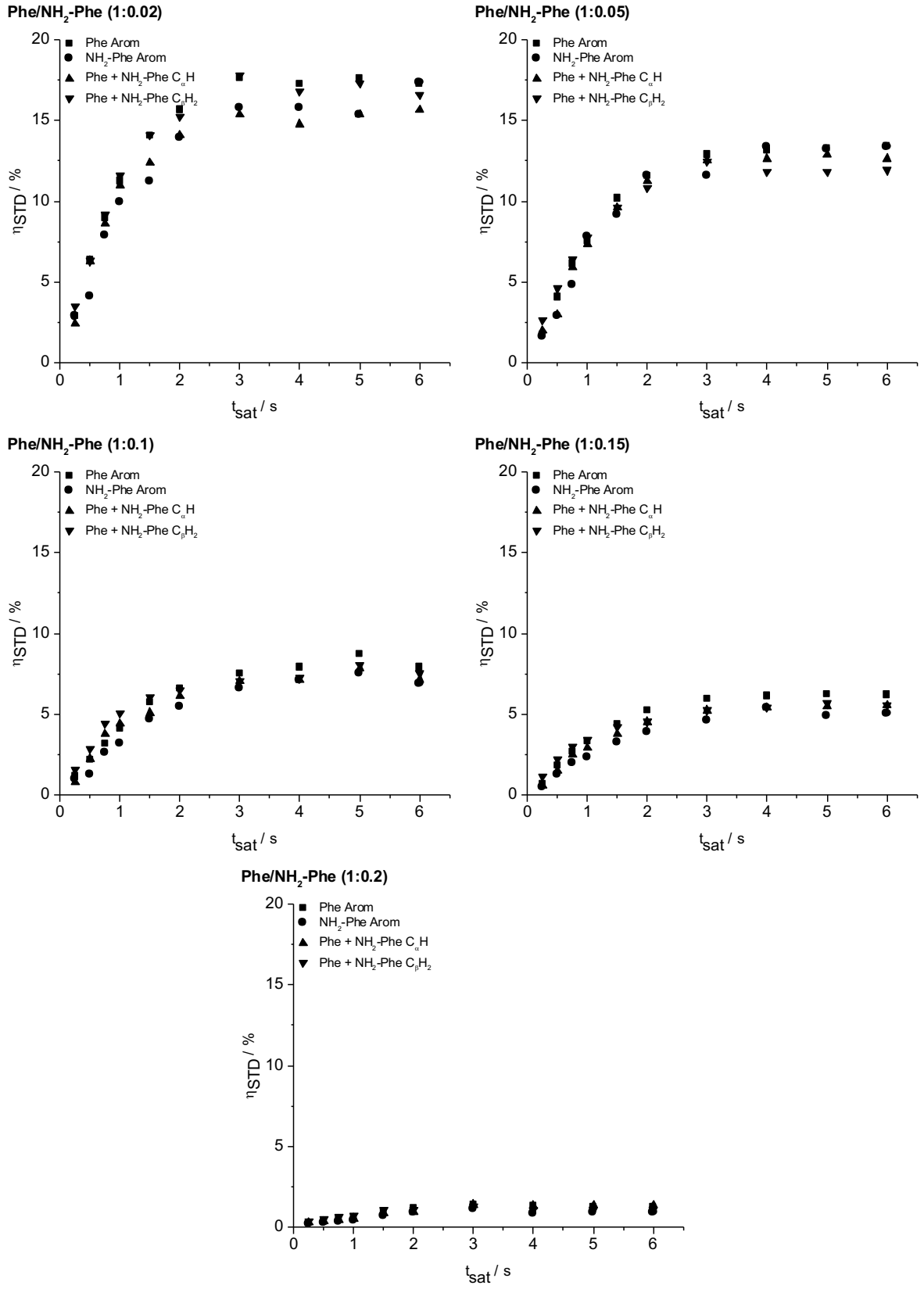

Figure S21. Evolution of fractional STD response (η_{STD}) for Phe/NH_2-Phe (1:0.02), Phe/NH_2-Phe (1:0.05), Phe/NH_2-Phe (1:0.1), Phe/NH_2-Phe (1:0.15) and Phe/NH_2-Phe (1:0.2) hydrogels measured at 298 K.

5.2.4. 2D ^{1}H-^{1}H NOESY experiments

No intermolecular spatial correlations were found between Phe and NH_2-Phe in the 2D ^{1}H-^{1}H NOESY spectrum of Phe/NH_2-Phe (1:1) solution (Figure S22).

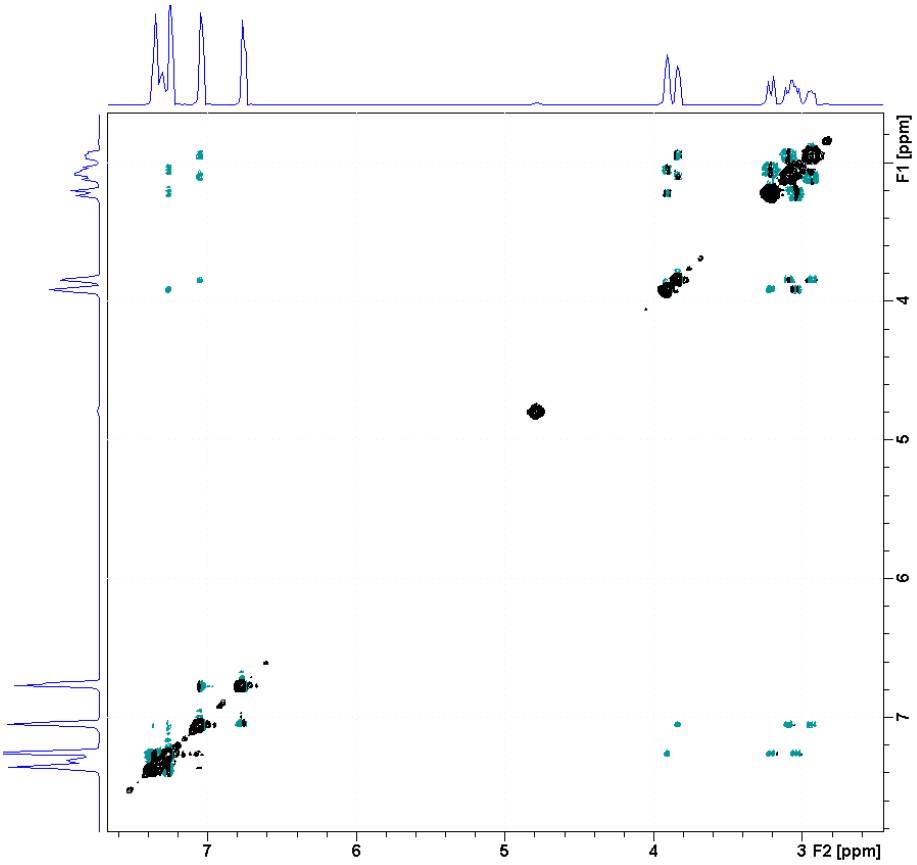

Figure S22. 2D ^{1}H-^{1}H NOESY NMR spectrum of Phe/NH_2-Phe (1:1) solution with a mixing time 1 s, acquired at 298 K.

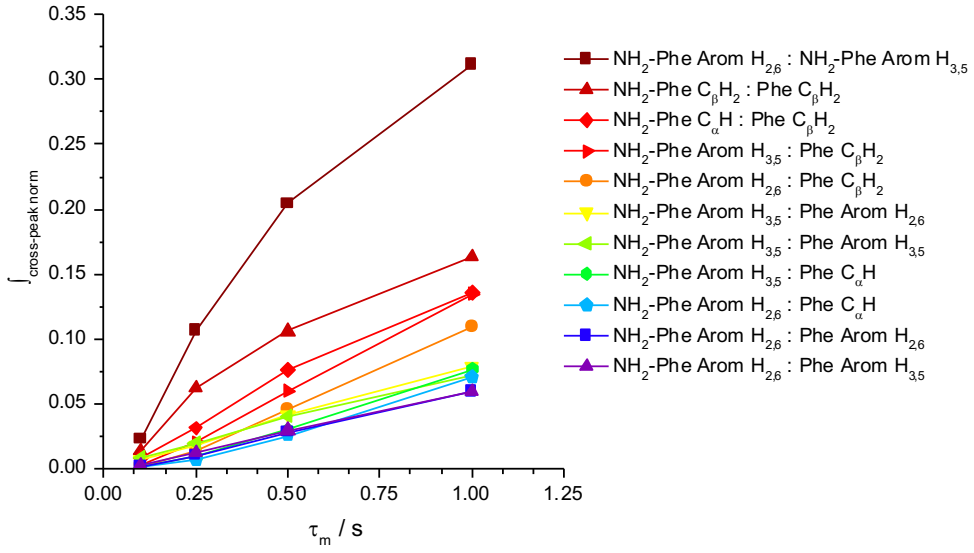

Figure S23. Evolution of normalised cross-peak intensity ($\int_{\text{cross-peak norm}}$) with mixing time in 2D ^{1}H-^{1}H NOESY NMR spectra of Phe/NH_2-Phe (1:0.15) hydrogel. Colour represents the degree of nOe enhancement.

References

[1] G. Yu, X. Yan, C. Han, F. Huang, *Chemical Society Reviews* **2013**, *42*, 6697-6722.

[2] S. M. Ramalhete, K. P. Nartwoski, N. Sarathchandra, J. S. Foster, A. N. Round, J. Angulo, G. O. Lloyd, Y. Z. Khimyak, *Chemistry-A European Journal* **2017**.

[3] B. Escuder, M. LLusar, J. F. Miravet, *The Journal of Organic Chemistry* **2006**, *71*, 7747-7752; M. D. Segarra-Maset, B. Escuder, J. F. Miravet, *Chemistry–A European Journal* **2015**, *21*, 13925-13929.